JACS
JOURNAL OF THE AMERICAN CHEMICAL SOCIETY
Article
pubs.acs.org/JACS

A Critical Size for Emergence of Nonbulk Electronic and Geometric Structures in Dodecanethiolate-Protected Au Clusters

Yuichi Negishi,*[,†,‡] Tafu Nakazaki,[†] Sami Malola,[§] Shinjiro Takano,[∥] Yoshiki Niihori,[†] Wataru Kurashige,[†] Seiji Yamazoe,[∥,⊥] Tatsuya Tsukuda,*[,∥,⊥] and Hannu Häkkinen*[,§,#]

[†]Department of Applied Chemistry, Faculty of Science, Tokyo University of Science, 1-3 Kagurazaka, Shinjuku-ku, Tokyo 162-8601, Japan

[‡]Photocatalysis International Research Center, Tokyo University of Science, 2641 Yamazaki, Noda, Chiba 278-8510, Japan

[§]Departments of Physics and [#]Chemistry, Nanoscience Center, University of Jyväskylä, FI-40014 Jyväskylä, Finland

[∥]Department of Chemistry, School of Science, The University of Tokyo, 7-3-1 Hongo, Bunkyo-ku, Tokyo 113-0033, Japan

[⊥]Elements Strategy Initiative for Catalysts and Batteries (ESICB), Kyoto University, Katsura, Kyoto 615-8520, Japan

Supporting Information

ABSTRACT: We report on how the transition from the bulk structure to the cluster-specific structure occurs in *n*-dodecanethiolate-protected gold clusters, $Au_n(SC12)_m$. To elucidate this transition, we isolated a series of $Au_n(SC12)_m$ in the *n* range from 38 to ~520, containing five newly identified or newly isolated clusters, $Au_{104}(SC12)_{45}$, $Au_{\sim226}(SC12)_{\sim76}$, $Au_{\sim253}(SC12)_{\sim90}$, $Au_{\sim356}(SC12)_{\sim112}$, and $Au_{\sim520}(SC12)_{\sim130}$, using reverse-phase high-performance liquid chromatography. Low-temperature optical absorption spectroscopy, powder X-ray diffractometry, and density functional theory (DFT) calculations revealed that the Au cores of $Au_{144}(SC12)_{60}$ and smaller clusters have molecular-like electronic structures and non-fcc geometric structures, whereas the structures of the Au cores of larger clusters resemble those of the bulk gold. A new structure model is proposed for $Au_{104}(SC12)_{45}$ based on combined approach between experiments and DFT calculations.

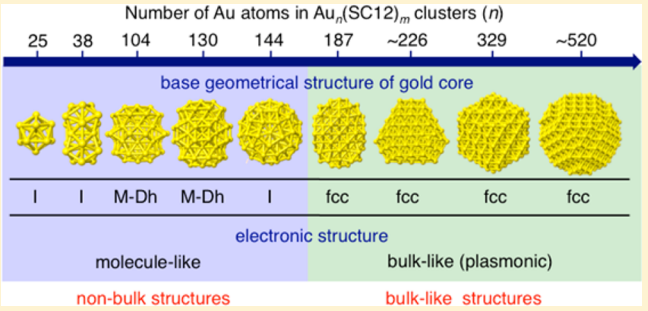

1. INTRODUCTION

Thiolate-protected gold clusters ($Au_n(SR)_m$) have attracted considerable attention as new functional nanomaterials because they exhibit specific and nonscalable physicochemical properties that are not seen in the gold nanoparticles and bulk gold.[1,2] To develop cluster-based materials by taking advantage of their unique properties, it is important to establish the critical size below which novel properties emerge. Detailed and systematic understanding on the structures has been attained for the phenylethanethiolate (SC2Ph)-protected Au clusters thanks to the atomically precise synthesis developed in the past decade.[3−15] Single crystal X-ray diffraction (XRD) revealed that $Au_{25}(SC2Ph)_{18}$ and $Au_{38}(SC2Ph)_{24}$ have icosahedral (Ic)-based Au cores.[3−5] Powder XRD and High-angle annular dark field scanning tunneling microscopy (HAADF-STEM) measurements with the help of density functional theory (DFT) calculations suggested Marks decahedral (M-Dh)-based or Ic-based Au cores for $Au_{67}(SC2Ph)_{35}$,[6] $Au_{103-105}(SC2Ph)_{45-46}$,[7] $Au_{130}(SC2Ph)_{50}$,[8] $Au_{137}(SC2Ph)_{56}$,[9] and $Au_{144}(SC2Ph)_{60}$,[10] and face-centered cubic (fcc) or M-Dh-based Au cores for larger clusters, $Au_{329}(SC2Ph)_{84}$,[11] $Au_{\sim500}(SC2Ph)_{\sim120}$,[13] and $Au_{\sim940}(SC2Ph)_{\sim160}$.[14] The small clusters have quantized, molecular-like electronic structures as evidenced by optical gaps and sharp peaks in the optical spectra. In contrast, the larger clusters show localized surface plasmon resonance (LSPR) band, suggesting that the confined electrons behave similarly to those of bulk-like Au nanoparticles.[3−15] These studies show that the transition in the geometric and electronic structures occur in the size range between $Au_{144}(SC2Ph)_{60}$ and $Au_{329}(SC2Ph)_{84}$. To understand the transition behavior, it is required to prepare a series of Au clusters with finely tuned sizes over a wide size range.

Contrary to the non-fcc Au cores in small $Au_n(SC2Ph)_m$, it has been reported that small Au clusters take fcc structures when protected by bulky thiolates, such as *c*-pentanethiolate (S*c*-C5), *c*-hexanethiolate (S*c*-C6), adamantine thiolate (SAdm), phenylthiolate (SPh), *t*-butylphenylthiolate (SPh-^{t}Bu), *t*-butylthiolate (S-^{t}Bu), and 3-mercaptobenzoic acid ($SPhCO_2H$). For example, the formation of fcc Au cores has been demonstrated by single-crystal XRD analyses of $[Au_{23}(Sc\text{-}C6)_{16}]^-$,[16] $Au_{24}(SAdm)_{16}$,[17] $Au_{28}(SPh\text{-}^tBu)_{20}$,[18] $Au_{30}S(S\text{-}^tBu)_{18}$,[19,20] $Au_{36}(SPh\text{-}^tBu)_{24}$,[21] $Au_{36}(Sc\text{-}C5)_{24}$,[22] $Au_{36}(SPh)_{24}$,[23] and by the low-dose electron microscopy of $Au_{68}(SPhCO_2H)_{32}$.[24] The formation of small fcc Au cores is probably due to steric effects associated with the bulky and rigid structures of thiolates. Thus, the second requirement to study the transition behavior is to use the proper thiolates that do

Received: October 25, 2014
Published: December 30, 2014

DOI: 10.1021/ja5109968
J. Am. Chem. Soc. 2015, 137, 1206−1212

not affect the intrinsic structures of the Au cores of $Au_n(SR)_m$.[25,26]

In this study, we investigated the structural transition of Au clusters protected by *n*-dodecanethiolate (SC12); C12S has long been used as a prototypical ligand[27−30] and does not affect the intrinsic nature of Au cores due to small steric effect. The clusters isolated and identified so far include $Au_{25}(SC12)_{18}$, $Au_{38}(SC12)_{24}$, $Au_{102}(SC12)_{44}$, $Au_{130}(SC12)_{50}$, $Au_{144}(SC12)_{60}$, $Au_{187}(SC12)_{68}$, and $Au_{329}(SC12)_{84}$.[11,29−31] In this work, we isolated 10 samples of molecularly pure $Au_n(SC12)_m$ including five newly identified or newly isolated clusters in the *n* range from 38 to ∼520 using reverse-phase high-performance liquid chromatography (HPLC).[31] The electronic structures of a series of well-defined $Au_n(SC12)_m$ were studied by temperature-dependent optical spectroscopy. The low-temperature optical absorption spectra show a clear transition from bulk-like (plasmonic) to molecule-like behavior between $Au_{187}(SC12)_{68}$ and $Au_{144}(SC12)_{60}$. Combined studies using powder XRD and DFT calculations revealed that the transition from fcc to non-fcc (icosahedral-based or M-Dh-based) structures occurs in the same size range.

2. EXPERIMENTAL AND COMPUTATIONAL METHODS

2.1. Chemicals. All chemicals were obtained commercially and were used without further purification. Hydrogen tetrachloroaurate tetrahydrate ($HAuCl_4{\cdot}4H_2O$) was obtained from Tanaka Kikinzoku. 1-Dodecanethiol (C12SH), 1-octanethiol (C8SH), tetraoctylammonium bromide (TOABr), sodium tetrahydroborate ($NaBH_4$), methanol, acetone, dichloromethane, and toluene were purchased from Wako Pure Chemical Industries. *trans*-2-[3-(4-*tert*-Butylphenyl)-2-methyl-2-propenylidene]malononitrile (DCTB) was purchased from Santa Cruz Biotechnology. Tetrabutylammonium perchlorate ($TBAClO_4$) was purchased from Tokyo Kasei. Deionized water with a resistivity above 18.2 MΩ cm was used.

2.2. Preparation of a Crude Sample. The crude sample of $Au_n(SC12)_m$ was prepared using the two-phase method.[32,33] A toluene solution (90 mL) of TOABr (5.5 mM, 0.5 mmol) was added to 90 mL of a $HAuCl_4$ aqueous solution (5 mM, 0.45 mmol). The mixture was stirred vigorously for 30 min at room temperature, after which the aqueous phase was removed. C12SH was added to the toluene solution ($[AuCl_4^-]/[C12SH]$ = 1:1, 0.45 mmol). The resultant solution was stirred vigorously at room temperature for 30 min and then at 0 °C for another 30 min. An aqueous solution of $NaBH_4$ (50 mM, 90 mL) cooled to 0 °C was added to the toluene solution. The solution changed color immediately from orange to dark brown. The solution was stirred for 3 h, washed three times with water cooled to 0 °C, and then dried in an evaporator. Methanol was added to the product, and C12SH, TOABr, and other byproducts were removed. A mixture of $Au_n(SC12)_m$ (100−120 mg) was obtained by this method.

The $Au_n(SC12)_m$ thus prepared transformed into $Au_n(SC12)_m$ with a high resistance to thiol etching by reaction with an excess of C12SH in air. An organic synthesizer (EYELA, PPS-2510) was used to control the reaction temperature precisely and reproducibly. $Au_n(SC12)_m$ (100 mg) was incubated in 6 mL of a thiol/toluene (1:1, v/v) mixture for 24 h at 80 °C. The amount of thiol used for incubation was less than that used in previous experiments,[31] resulting in gentle etching conditions and an increase in the variety of resultant $Au_n(SC12)_m$. After reaction, methanol was added to the product, and C12SH and byproducts were removed. Finally, 80−90 mg of stable clusters was obtained.

The octanethiolate-protected $Au_n(SC8)_m$ was also synthesized in this study for comparison purpose by using the same experimental procedures, except that C8SH was used instead of C12SH.

2.3. Chromatographic Separation. The resultant $Au_n(SC12)_m$ was fractionated by HPLC (Japan Analytical Industry Co., Ltd., LC-9201) according to cluster size. Two stainless-steel reverse-phase columns (BDS Hypersil C8 stationary phase 250 × 21.2 mm inner diameter and BDS Hypersil Phenyl 150 × 21.2 mm inner diameter, both with 5 μm particles) connected in series (C8 column first) were used in the HPLC apparatus.[31,34−36] The mobile phase was 10 mM $TBAClO_4/CH_2Cl_2$ and had a flow rate of 4.5 mL min^{-1}. The chromatogram was collected by measuring the absorption at 290 nm. Clusters with concentrations less than 10 mg/mL were injected into the columns during a typical operation. Samples of $Au_n(SC8)_m$ for comparison purpose were also separated in the same experimental condition.

2.4. Characterization. Laser desorption ionization (LDI) mass spectra were obtained using a spiral time-of-flight mass spectrometer (JEOL Ltd., JMS−S3000) and semiconductor laser (349 nm). Matrix-assisted laser desorption ionization (MALDI) mass spectra were collected using a reflectron-type time-of-flight mass spectrometer (Bruker, UltraFLEX II) using a nitrogen laser (wavelength: 337 nm). In the MALDI experiments, DCTB was used as the matrix.[37] The cluster-to-matrix ratio was set to 1:1000. Electrospray ionization (ESI) time-of-flight mass spectra were recorded using a custom-designed mass spectrometer.[38] A 1 mg/mL toluene/acetonitrile solution (7:3, v/v) of $Au_n(SC12)_m$ was electrosprayed at 240 μL/h. The charged liquid droplets were fed into a capillary and heated resistively to ∼180 °C to form intact cluster ions via desolvation. High-resolution ESI mass spectrometry was performed using a Fourier-transform mass spectrometer (Bruker, Solarix). A 1 mg/mL of toluene/acetonitrile (1:1, v:v) solution of $Au_n(SC12)_m$ was electrosprayed at a flow rate of 800 μL/h.

Transmission electron microscopy (TEM) images were recorded using an electron microscope (Hitachi, H-9500) operating at 200 kV, typically with a magnification of 150 000. The histogram of the core diameter for each fraction was made by measuring the sizes of >300 particles.

X-ray photoelectron spectra were collected using an electron spectrometer (JEOL, JPS-9010MC) operated at a base pressure of ∼2 × 10^{-8} Torr. X-rays from the Mg Kα line at 1253.6 eV were used for photoemission.

Thermogravimetric analysis (TGA; Bruker, TGA2000SA) was performed using ∼4 mg samples of $Au_n(SC12)_m$ at a heating rate of 5 °C/min under N_2 flow over the temperature range 25−500 °C.

XRD measurements were performed on a Rigaku Rint2500 using Cu Kα radiation (λ = 1.5418 Å). The reflection-free silicon plate was used as a substrate. The raw XRD data, which are functions of θ, were converted to s (= $2\sin\theta/\lambda$)-dependent data. In this process, the intensity was corrected on the basis of Jacobian factor.[28]

Temperature-controlled optical absorption spectra were recorded at 290−25 K by using a spectrometer (Ocean Optics Inc., HR-4000CG-UV-NIR) with optical fibers. The filmed samples were prepared as follows. A toluene solution of each cluster (ca. 5 mg/mL) was placed onto a calcium fluoride (CaF_2) plate (Ohyo Koken Kogyo Co., Ltd, 15 × 15 × 1 mm) and the solvent was evaporated slowly. This process was repeated until the homogeneous film with appropriate optical density was formed. The absorption spectra of the central portion of the film were acquired. The sample plate was placed in a ^{4}He cryostat (Iwatani Industrial Gases Corp., S030) with a Cu sample holder. The cryostat was evacuated by a turbo molecular pump (Pfeiffer Vacuum Inc., Hi Cube 80 Eco) and temperature of the sample was controlled with a resistive heater (Supporting Information Figure S1).

2.5. Computational Methods. We used the density functional theory (DFT) as implemented in the real-space code-package GPAW (Grid-based Projector-Augmented Wave method).[39,40] Structure optimization (see 3.5) was performed using the local density approximation (LDA) exchange-correlation functional,[41] 0.2 Å grid spacing, and 0.05 eV/Å convergence criterion for the maximum forces acting on atoms in clusters (Schemes S1−S9). LDA approximation is known to reproduce the gold−gold distances in the metal core better as compared to the higher-level functionals. The GPAW setups for gold include scalar-relativistic corrections. Optical absorption spectra were calculated for the LDA relaxed structures using Casida's formulation of the linear response time-dependent DFT[42,43] and PBE (Perdew−Burke−Ernzerhof) functional[44] in a real-space grid 0.25 Å spacing. Theoretical XRD patterns were calculated as described before in ref 45. This includes modeling the thermal damping by a Debye−Waller factor

DOI: 10.1021/ja5109968
J. Am. Chem. Soc. 2015, 137, 1206−1212

exp($-Bs^2/2$) where $s = 2\sin\theta/\lambda$ ($\lambda = 1.54$ Å) and $B = 0.04$ nm^2. The form factors for different atoms scale in proportion to their atomic numbers.

3. RESULTS AND DISCUSSION

3.1. Fractionation. Figure 1a shows the positive-ion LDI mass spectrum of a mixture of $Au_n(SC12)_m$. The ion intensities of

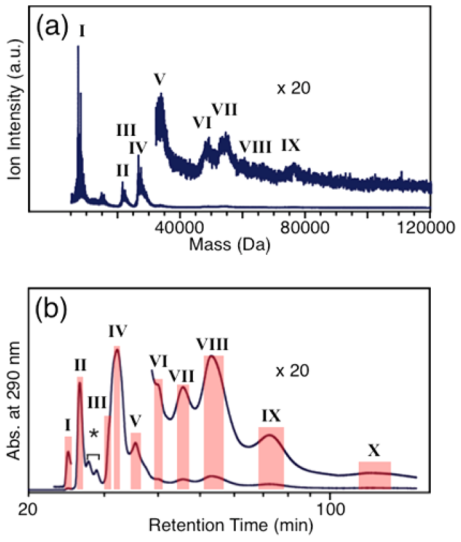

Figure 1. (a) Positive-ion LDI mass spectrum and (b) reverse-phase HPLC chromatogram of a crude sample of $Au_n(SC12)_m$.

large clusters are small in the mass spectrum probably due to smaller ionization and detection efficiency than smaller clusters. However, the enlarged mass spectrum indicates that a wide size range of $Au_n(SC12)_m$ were present in the crude sample.

Figure 1b shows a chromatogram of the crude sample of $Au_n(SC12)_m$ recorded by monitoring the absorption at 290 nm. The chromatogram contains multiple peaks, indicating that a mixture was separated successfully by reverse-phase HPLC. The relative intensity of each peak does not directly reflect the relative abundance of each cluster in the sample since the absorption coefficient depends on the cluster size.[13,14,38] Figure S2 (Supporting Information) shows the TEM images and the core size distributions of fractions **I**–**X**. All the fractions have a narrow core size distribution and the average core diameters increased monotonically in the order of **I** → **X** (Supporting Information Figure S2 and Table 1). These observations indicate that a series of $Au_n(SC12)_m$ have been separated clearly and systematically by reverse-phase HPLC.

We observed a small fraction labeled with an asterisk in Figure 1b between fractions **II** and **III**. Their retention times slightly changed in each experiment. LDI mass spectrometry of this fraction indicated the core mass was 15 kDa (data not shown). The mass analysis and the reported synthesis of $[Au_{67}(SR)_{35}]^{2-}$ (R = C2Ph or C6)[6] suggests that this fraction may be assigned to $[Au_{67}(SC12)_{35}]^{2-}$. Because the yield of this species was small, we did not study this compound further in the present study.

3.2. Chemical Compositions. The $Au_n(SC12)_m$ clusters in fractions **I**–**X** were characterized by LDI, MALDI, and ESI mass spectrometry in the positive-ion mode. LDI mass spectra (Figure 2) show that fractions **I**–**X** contain clusters with different core masses in the range of 8–108 kDa. The ESI mass spectra (Figure 3(a)) and MALDI mass spectra (Supporting Information Figure S3) of fractions **I**–**X** exhibit sharp peaks reflecting the high purity of the clusters in the fractions. The clusters in five fractions **I**, **III**–**V** and **VIII** can be assigned to $Au_{38}(SC12)_{24}$, $Au_{130}(SC12)_{50}$, $Au_{144}(SC12)_{60}$, $Au_{187}(SC12)_{68}$, and $Au_{329}(SC12)_{84}$, respectively (Table 1), which have been reported previously.[11,30,31]

Fraction **II** has been assigned to $Au_{102}(SC12)_{44}$ in our previous paper[31] based on low-resolution ESI mass spectra and on the chemcial composition of the well-known magic cluster, $Au_{102}(p\text{-MBA})_{44}$ (*p*-MBA = *p*-mercaptobenzoic acid).[46] However, the comparison of the high-resolution ESI mass spectra of fraction **II** (Figure 3(b)) and the corresponding fraction of C8S-protected Au clusters (Supporting Information Figure S4) lead us to correct the chemical composition of the clusters in **II** to be $Au_{104}(SC12)_{45}$. This new chemical composition has not been

Table 1. Compositions of Fractions I–X, VI′, VII′, IX′, and X′

fraction[a]	M_w[b]	chemical composition	core mass (kDa)[c]	D (nm)[d]
I	12,318	$Au_{38}(SC12)_{24}$	8	1.1 ± 0.1
II	29,547	$Au_{104}(SC12)_{45}$	21	1.4 ± 0.3
III	35,675	$Au_{130}(SC12)_{50}$	26	1.5 ± 0.3
IV	40,447	$Au_{144}(SC12)_{60}$	29	1.6 ± 0.1
V	50,528	$Au_{187}(SC12)_{68}$	38	1.8 ± 0.3
VI	~59,820	$Au_{\sim226}(SC12)_{\sim76}$	45	2.0 ± 0.5
VII	~68,000	$Au_{\sim253}(SC12)_{\sim90}$	53	2.1 ± 0.4
VIII	~81,760	$Au_{329}(SC12)_{84}$	66	2.2 ± 0.4
IX	~92,630	$Au_{\sim356}(SC12)_{\sim112}$	75	2.2 ± 0.3
X	~128,700	$Au_{\sim520}(SC12)_{\sim130}$	108	2.4 ± 0.2
VI′	~55,570	$Au_{\sim226}(SC8)_{\sim76}$	46	–
VII′	~62,940	$Au_{\sim253}(SC8)_{\sim90}$	53	–
IX′	~86,350	$Au_{\sim356}(SC8)_{\sim112}$	75	–
X′	~121,300	$Au_{\sim520}(SC8)_{\sim130}$	108	–

[a]Fractions **VI′**, **VII′**, **IX′** and **X′** were obtained by the fractionation of $Au_n(SC8)_m$ (Supporting Information Figure S5). [b]Molecular weights obtained by the deconvolution of ESI mass spectra. The molecular weights of **I**–**V** were determined using high-resolution ESI FT-ICR mass spectrometer and those of **VI**–**X** and **VI′**–**X′** were evaluated using homemade ESI TOF mass spectrometer because their molecular weights are over the range of ESI FT-ICR mass spectrometer. [c]The peak position observed in LDI mass spectra. [d]Diameters obtained by TEM measurements.

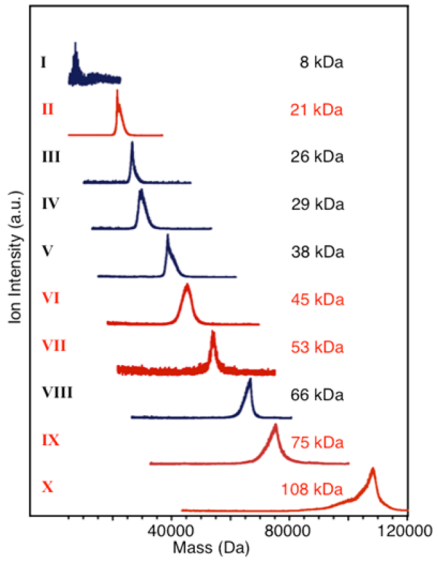

Figure 2. Positive-ion LDI mass spectra of fractions **I**–**X**. Fractions containing newly identified clusters (**II**) and newly isolated clusters (**VI**, **VII**, **IX**, and **X**) are shown in red.

DOI: 10.1021/ja5109968
J. Am. Chem. Soc. 2015, 137, 1206–1212

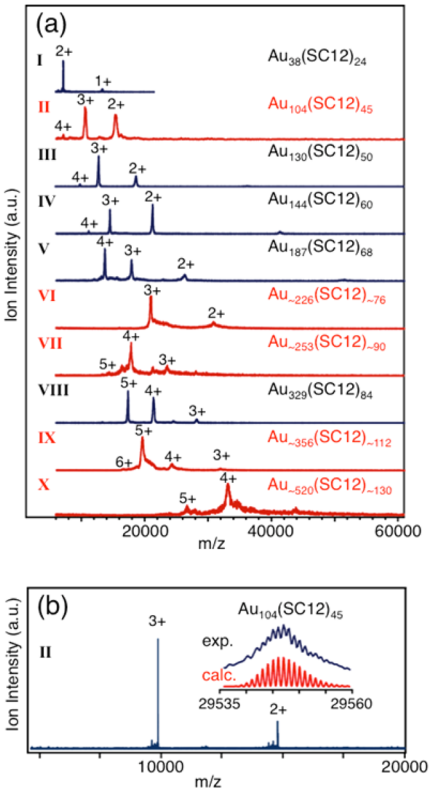

Figure 3. (a) Low-resolution positive-ion ESI mass spectra of fractions **I**–**X** and (b) high-resolution positive-ion ESI mass spectrum of fractions **II**. Inset shows the deconvoluted spectrum for 2+ with the calculated isotope pattern for $Au_{104}(SC12)_{45}$.

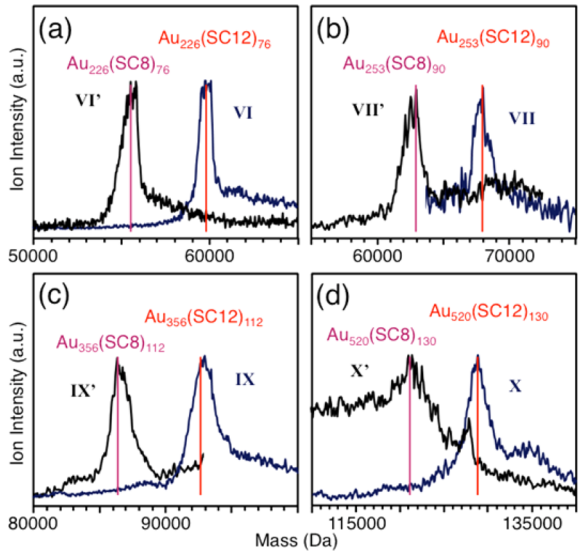

Figure 4. Comparison of deconvoluted ESI mass spectra between $Au_n(SC12)_m$ (fractions (a) **VI**, (b) **VII**, (c) **IX**, and (d) **X**) and $Au_n(SC8)_m$ (fractions (a) **VI**′, (b) **VII**′, (c) **IX**′ and (d) **X**′: Supporting Information Figure S5 and Table 1).

reported for alkanethiolate-protected Au clusters, while $Au_{104}(SC2Ph)_{45}$ was reported.[7]

The LDI mass spectra of the other four fractions **VI**, **VII**, **IX** and **X** exhibit the broad peaks at the masses of 45, 53, 75, and 108 kDa, respectively (Figure 2 and Table 1). The clusters in **VI**, **VII**, and **X** presumably correspond to previously reported alkanethiolate-protected Au clusters with the core masses of 46 kDa,[27] 57 kDa,[27] and 100 kDa,[28] respectively. The cluster in **VI** and **X** may correspond to $Au_{225}(SC6)_{75}$ assigned using nonmass spectrometric methods (TEM and thermogravimetric analysis)[34] and $Au_{\sim500}(SC2Ph)_{\sim120}$ assigned using ESI mass spectrometry,[13] respectively. However, the compositions of these clusters have not been identified in the $Au_n(SC12)_m$ so far. The clusters in **IX** have not been reported previously.

The chemical compositions of the clusters in **VI**, **VII**, **IX**, and **X** were determined more precisely by comparing their ESI mass spectra with those in **VI**′, **VII**′, **IX**′, and **X**′ of $Au_n(SC8)_m$ with the same core masses of 46, 53, 75, and 108 kDa, respectively (Supporting Information Figure S5). Figure 4 shows the comparison of deconvoluted ESI mass spectra between $Au_n(SC12)_m$ and $Au_n(SC8)_m$. These comparisons enabled us to determine the number of thiolate ligands and then the number of gold atoms can be determined from the total molecular weight (M_w).[6,9,11,13,14,30,31,38] For example, the difference in the molecular weights between **VI** and **VI**′ (Table 1) is ~4250 Da (Figure 4a). This value corresponds to ~76-fold of the difference in the molecular weights between SC_8H_{17} and $SC_{12}H_{25}$ (56 Da) ($56 \times 76 = 4256$), meaning that the clusters in **VI** and **VI**′ contain the 76 thiolate ligands. The subtraction of the weight of the ligands from the molecular weights of the cluster enables us to determine the number of Au atoms to be 226 ({[59820 − (201 × 76)] ÷ 197} = 226.1). On the basis of these comparisons, the chemical compositions of the clusters in fractions **VI**, **VII**, **IX**, and **X** were determined to be $Au_{\sim226}(SC12)_{\sim76}$, $Au_{\sim253}(SC12)_{\sim90}$, $Au_{\sim356}(SC12)_{\sim112}$, and $Au_{\sim520}(SC12)_{\sim130}$, respectively (Table 1). Note that $Au_{225}(SC6)_{75}$ proposed previously[34] has a M_w of 59 400 and does not explain the M_w (59 820) of the clusters in **VI**. Although the chemical compositions thus estimated are supported by TG analysis (Supporting Information Figure S6), there is an ambiguity in the compositions due to limited mass resolution of the mass spectrometer used in this work (Figure 4). Thus, we describe the number of the gold atoms and thiolates with the notation of "~" in this manuscript. The Au 4f and S 2p X-ray photoelectron spectra of newly identified clusters in **VI**, **VII**, **IX**, and **X** are presented in Supporting Information Figures S7 and S8, respectively.

3.3. Evolution of Electronic Structure. Figure 5 shows the temperature dependent optical absorption spectra of the filmed samples of **I**–**X**. In the spectra of **I**–**IV**, the peaks become sharper and more intense and the peak positions are blue-shifted with decreasing temperature. Similar phenomena were reported for $Au_{25}(SC2Ph)_{18}$, $Au_{38}(SC2Ph)_{24}$, and $Au_{144}(SC6)_{60}$.[47,48] The spectral changes at lower temperature were explained in terms of decreased interactions between electrons or excitons within the Au core and phonons at the staple.[47] These results indicate that clusters **I**–**IV** have discrete electronic structures. On the other hand, the optical absorption spectra of **V**–**X** exhibit a distinct peak in the 520–540 nm range assignable to LSPR band. The intensity and position of the LSPR band did not change appreciably even at 25 K, which is consistent with previous studies.[49,50] These results demonstrate that the clusters in **V**–**X** no longer have discrete electronic structures. We therefore conclude that the transition of electronic structures occur between $Au_{144}(SC12)_{60}$ and $Au_{187}(SC12)_{68}$.

3.4. Evolution of Geometric Structure. Structural evolution of $Au_n(SC12)_m$ was studied by powder XRD. Figure 6 shows the powder XRD patterns of **I**–**X**. The XRD patterns of **I** ($Au_{38}(SC12)_{24}$), **II** ($Au_{104}(SC12)_{45}$), **IV** ($Au_{144}(SC12)_{60}$), **VI** ($Au_{\sim226}(SC12)_{\sim76}$), **VIII** ($Au_{329}(SC12)_{84}$) are consistent with

DOI: 10.1021/ja5109968
J. Am. Chem. Soc. 2015, 137, 1206–1212

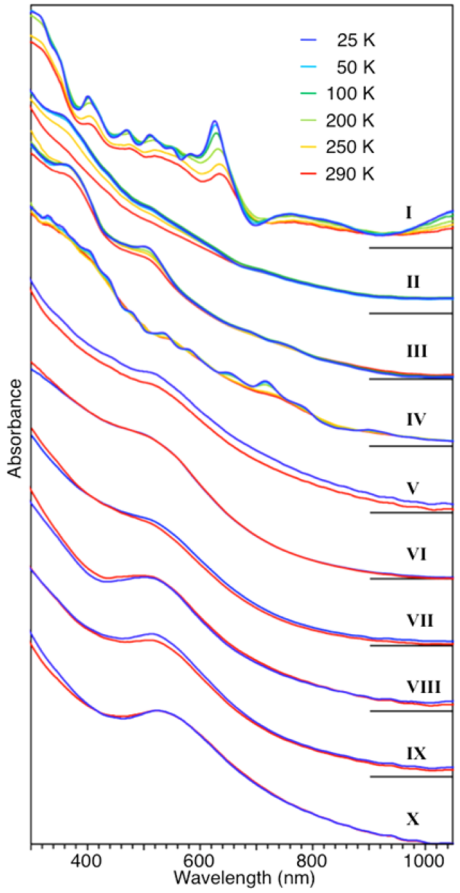

Figure 5. Temperature dependence of optical absorption spectra of the filmed samples of $Au_n(SC12)_m$.

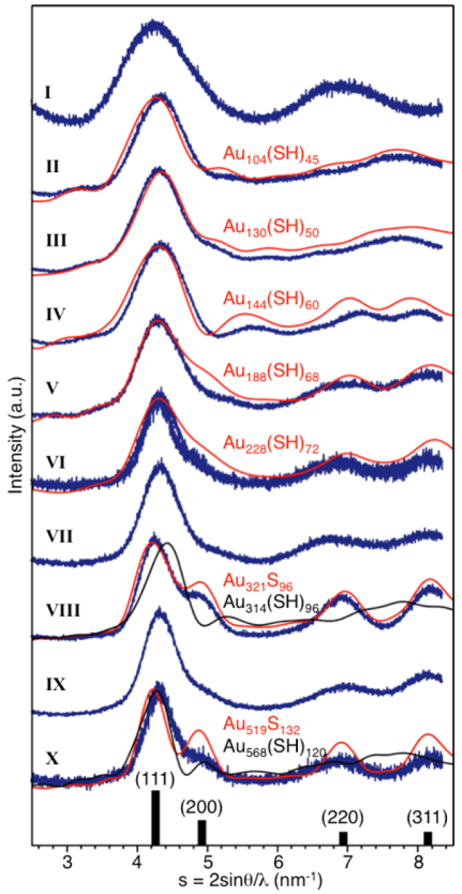

Figure 6. Powder XRD patterns of $Au_n(SC12)_m$. The calculated XRD patterns of the model structures are also shown by red or black lines. The black vertical bars indicate the peak positions of bulk Au.

early reports by Whetten group, where each cluster was described as 8, 22, 29, 46, 65 kDa clusters, respectively.[28,51,52] The broad XRD pattern of **I** ($Au_{38}(SC12)_{24}$) is consistent with those of $Au_{38}(SC2Ph)_{24}$, which has a face-fused biicosahedral Au_{23} core.[5,53] In **IV**, the small peaks appeared at s = ~5.5, ~7, and ~8 nm^{-1}, whereas the first peak at s = ~5.5 nm^{-1} disappeared in larger clusters. At the same time, a small peak or shoulder corresponding to the diffraction from the (220) planes became prominent in larger clusters **V**–**X**. These trends suggest that the clusters **V**–**X** have fcc Au cores.

3.5. Structure Models. Structural models of small clusters in **II**–**IV** are provided by DFT calculations. Since DFT computations are very CPU-intensive for the size range studied here, we considered the model structures using SH instead of SC12. The structures of $Au_{104}(SH)_{45}$, $Au_{130}(SH)_{50}$, and $Au_{144}(SH)_{60}$ optimized by DFT calculations are shown in Figure 7a. $Au_{104}(SH)_{45}$ has a Au_{79} M-Dh core similar to that found in $Au_{102}(p\text{-MBA})_{44}$.[46] The $Au_{130}(SH)_{50}$ has a Au_{105} core constructed by adding atomic layers along the five-fold axis of the Au_{79} M-Dh core of $Au_{104}(SH)_{45}$.[31,54] The $Au_{144}(SH)_{60}$ is based on the model predicted by Lopez-Acevedo et al. and has an Ic-based Au_{114} core consisting of two Mackay (M) Ic shells and one anti-Mackay (AM) layer (12 + 42 + 60 atoms).[45] In the "Divide and Protect"[55] scheme, these clusters can be formulated as $Au_{79}[Au_2(SH)_3]_5[Au(SH)_2]_{15}$, $Au_{105}[Au(SH)_2]_{25}$, and $Au_{114}[Au(SH)_2]_{30}$, respectively.

In Figure 7b, the optical absorption spectra of fractions **II** ($Au_{104}(SC12)_{45}$), **III** ($Au_{130}(SC12)_{50}$), and **IV** ($Au_{144}(SC12)_{60}$) recorded at 25 K are compared with those calculated for $Au_{104}(SH)_{45}$, $Au_{130}(SH)_{50}$, and $Au_{144}(SH)_{60}$. Overall, the agreement is good given that the dodecanethiolate is simplified to SH (Figure 7a). Particularly striking is the case of Au_{144}: our calculated spectrum reproduces seven features in the low-temperature experimental spectrum between 400 and 750 nm. In Figure 6, the XRD patterns simulated for $Au_{104}(SH)_{45}$, $Au_{130}(SH)_{50}$, and $Au_{144}(SH)_{60}$ are superimposed with those of **II**–**IV**, respectively. The agreement between experiment and theory is again very good. Thus, we conclude that the Au cores of $Au_{104}(SC12)_{45}$, $Au_{130}(SC12)_{50}$, and $Au_{144}(SC12)_{60}$ have the M-Dh, M-Dh, and Ic-based structures, respectively (Figure 7(a)). Similar conclusions have been made on $Au_{103-105}(SC2Ph)_{45-46}$, $Au_{130}(SC2Ph)_{50}$ and $Au_{144}(SC2Ph)_{60}$.[7,8,45,56] Combined with the good level of agreement between theory and experiment, these results indicate that our predicted structures for $Au_{104}(SR)_{45}$, $Au_{130}(SR)_{50}$, and $Au_{144}(SR)_{60}$ should be realistic.

For larger clusters, it is not trivial to determine the global minimum structures because of many possible structures and absence of structure-sensitive properties. In the present work, we attempted to determine whether the cores of the clusters in selected fractions **VIII** ($Au_{329}(SC12)_{84}$) and **X** ($Au_{\sim520}(SC12)_{\sim130}$) are fcc or Ic by simulating XRD patterns of model structures having comparable compositions as those isolated experimentally. Ic-based models have been constructed by adding shells onto the Au_{114} core of $Au_{144}(SH)_{60}$. As a result, we obtained $Au_{314}(SH)_{96}$ with an Ic-based Au_{266} core consisting of three M shells and one AM layer (12 + 42 + 92 + 120 atoms).[57] Similarly, $Au_{568}(SH)_{120}$ having an Ic-based Au_{508} core consisting

DOI: 10.1021/ja5109968
J. Am. Chem. Soc. 2015, 137, 1206–1212

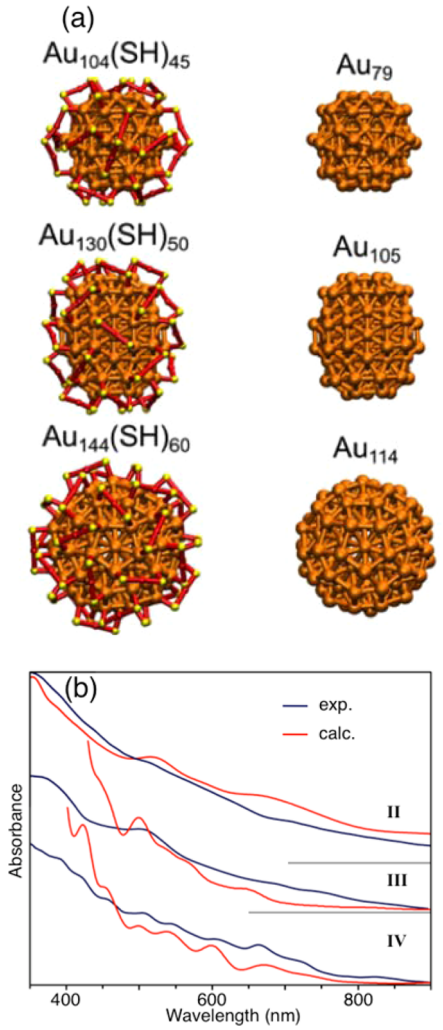

Figure 7. (a) Optimized structures of $Au_{104}(SH)_{45}$, $Au_{130}(SH)_{50}$, and $Au_{144}(SH)_{60}$. Both the full model and the corresponding gold core are shown. Orange, gold; red, ligand units containing Au(I); yellows sulfur. Hydrogen is not shown. (b) Comparison of optical spectra of **II**–**IV** at 25 K and calculated for $Au_{104}(SH)_{45}$, $Au_{130}(SH)_{50}$, and $Au_{144}(SH)_{60}$. In the calculated spectra, the individual optical transitions are broadened by a 0.1 eV Gaussian for $Au_{104}(SH)_{45}$ and by 0.05 eV Gaussian for $Au_{130}(SH)_{50}$ and $Au_{144}(SH)_{60}$. The Au_{104} spectrum was calculated for singly charged cation cluster corresponding to a filled 58 electron shell.

of four M shells and one AM layer (12 + 42 + 92 + 162 + 198 atoms) was obtained. These two models are possible candidates for $Au_{329}(SC12)_{84}$ and $Au_{\sim520}(SC12)_{\sim130}$, respectively. In contrast, we considered $Au_{321}S_{96}$ and $Au_{519}S_{132}$ clusters with Au_{273} and Au_{453} cores with fcc structures as alternative candidates for $Au_{329}(SC12)_{84}$ and $Au_{\sim520}(SC12)_{\sim130}$, respectively. The structures of $Au_n(SH)_m$ were optimized by DFT calculations, whereas those of Au_nS_m were not. The structure models used in the XRD analysis are shown in Supporting Information. Figure 6 compares the XRD patterns of **VIII** and **X** and the simulated results for the corresponding model structures. The four diffraction peaks due to (111), (200), (220), and (311) of **VIII** are reproduced by $Au_{321}S_{96}$ much better than $Au_{314}(SH)_{96}$. The XRD pattern of **X** is much more similar to that of $Au_{519}S_{132}$ than $Au_{568}(SH)_{120}$. These results indicate that the clusters in **VIII** ($Au_{329}(SC12)_{84}$) and **X** ($Au_{\sim520}(SC12)_{\sim130}$) have Au cores with fcc structures as in the case of $Au_{329}(SC2Ph)_{84}$, $Au_{\sim500}(SC2Ph)_{\sim120}$, and $Au_{\sim940}(SC2Ph)_{\sim160}$.[11−14] The XRD patterns of smaller clusters in **V** ($Au_{187}(SC12)_{68}$) and **VI** ($Au_{\sim226}(SC12)_{\sim76}$) were reproduced reasonably well with model structures $Au_{188}(SH)_{68}$ and $Au_{228}(SH)_{72}$ with fcc Au_{148} and Au_{189} cores, respectively.

4. CONCLUSION

We have succeeded in isolating a series of $Au_n(SC12)_m$ systematically, including five newly identified or newly isolated clusters, in the size region covering the critical region where molecular-like electronic structures and nonbulk geometric structures emerge. Optical spectroscopy and powder XRD analysis revealed that bulk-to-nonbulk transition of electronic and geometric transition occurs between $Au_{187}(SC12)_{68}$ and $Au_{144}(SC12)_{60}$. We also proposed realistic model structures for smaller clusters. $Au_{104}(SR)_{45}$, $Au_{130}(SR)_{50}$, and $Au_{144}(SR)_{60}$ have the Au_{79}, Au_{105}, and Au_{114} cores, respectively, with five-fold symmetry and quantized electronic structures. We expect that the structural information reported here will deepen our understanding of the origin of size-specific physical and chemical properties of $Au_n(SR)_m$.

■ ASSOCIATED CONTENT

Ⓢ Supporting Information

Supporting figures and description of the computational cluster models. This material is available free of charge via the Internet at http://pubs.acs.org.

■ AUTHOR INFORMATION

Corresponding Authors

negishi@rs.kagu.tus.ac.jp
tsukuda@chem.s.u-tokyo.ac.jp
hannu.j.hakkinen@jyu.fi

Notes

The authors declare no competing financial interest.

■ ACKNOWLEDGMENTS

We thank Mr. Masaki Yamaguchi, Mr. Yoshiki Matsuura, Ms. Miku Matsuzaki, Ms. Chihiro Uchida, Ms. Makoto Eguro, Mr. Ryota Tomizawa, Ms. Ayano Kato, Mr. Yoshihiro Kikuchi, and Mr. Tomohisa Murayama for technical assistance. The experimental work was supported financially by the Grants-in-Aid for Scientific Research (Nos. 25288009 and 25102539), the Canon Foundation, and the SEI Group CSR Foundation. The computational work was supported by the Academy of Finland, CSC − the Finnish IT Center for Science, and the Partnership for Advanced Computing in Europe (PRACE infrastructure).

■ REFERENCES

(1) Häkkinen, H. *Nat. Chem.* **2012**, *4*, 443−455.
(2) Tsukuda, T. *Bull. Chem. Soc. Jpn.* **2012**, *85*, 151−168.
(3) Heaven, M. W.; Dass, A.; White, P. S.; Holt, K. M.; Murray, R. W. *J. Am. Chem. Soc.* **2008**, *130*, 3754−3755.
(4) Zhu, M.; Aikens, C. M.; Hollander, F. J.; Schatz, G. C.; Jin, R. *J. Am. Chem. Soc.* **2008**, *130*, 5883−5885.
(5) Qian, H.; Eckenhoff, W. T.; Zhu, Y.; Pintauer, T.; Jin, R. *J. Am. Chem. Soc.* **2010**, *132*, 8280−8281.
(6) Nimmala, P. R.; Yoon, B.; Whetten, R. L.; Landman, U.; Dass, A. *J. Phys. Chem. A* **2013**, *117*, 504−517.
(7) Dass, A.; Nimmala, P. R.; Jupally, V. R.; Kothalawala, N. *Nanoscale* **2013**, *5*, 12082−12085.
(8) Jupally, V. R.; Dass, A. *Phys. Chem. Chem. Phys.* **2014**, *16*, 10473−10479.

DOI: 10.1021/ja5109968
J. Am. Chem. Soc. 2015, 137, 1206−1212

(9) Jupally, V. R.; Dharmaratne, A. C.; Crasto, D.; Huckaba, A. J.; Kumara, C.; Nimmala, P. R.; Kothalawala, N.; Delcamp, J. H.; Dass, A. *Chem. Commun.* **2014**, *50*, 9895−9898.
(10) Bahena, D.; Bhattarai, N.; Santiago, U.; Tlahuice, A.; Ponce, A.; Bach, S. B. H.; Yoon, B.; Whetten, R. L.; Landman, U.; Jose-Yacaman, M. *J. Phys. Chem. Lett.* **2013**, *4*, 975−981.
(11) Kumara, C.; Dass, A. *Anal. Chem.* **2014**, *86*, 4227−4232.
(12) Qian, H.; Zhu, Y.; Jin, R. *Proc. Natl. Acad. Sci. U.S.A.* **2012**, *109*, 696−700.
(13) Kumara, C.; Zuo, X.; Ilavsky, J.; Chapman, K. W.; Cullen, D. A.; Dass, A. *J. Am. Chem. Soc.* **2014**, *136*, 7410−7417.
(14) Kumara, C.; Zuo, X.; Cullen, D. A.; Dass, A. *ACS Nano* **2014**, *8*, 6431−6439.
(15) Qian, H.; Jin, R. *Nano Lett.* **2009**, *9*, 4083−4087.
(16) Das, A.; Li, T.; Nobusada, K.; Zeng, C.; Rosi, N. L.; Jin, R. *J. Am. Chem. Soc.* **2013**, *135*, 18264−18267.
(17) Crasto, D.; Barcaro, G.; Stener, M.; Sementa, L.; Fortunelli, A.; Dass, A. *J. Am. Chem. Soc.* **2014**, *136*, 14933−14940.
(18) Zeng, C.; Li, T.; Das, A.; Rosi, N. L.; Jin, R. *J. Am. Chem. Soc.* **2013**, *135*, 10011−10013.
(19) Yang, H.; Wang, Y.; Edwards, A. J.; Yan, J.; Zheng, N. *Chem. Commun.* **2014**, *50*, 14325−14327.
(20) Crasto, D.; Malola, S.; Brosofsky, G.; Dass, A.; Häkkinen, H. *J. Am. Chem. Soc.* **2014**, *136*, 5000−5005.
(21) Zeng, C.; Qian, H.; Li, T.; Li, G.; Rosi, N. L.; Yoon, B.; Barnett, R. N.; Whetten, R. L.; Landman, U.; Jin, R. *Angew. Chem., Int. Ed.* **2012**, *51*, 13114−13118.
(22) Das, A.; Liu, C.; Zeng, C.; Li, G.; Li, T.; Rosi, N. L.; Jin, R. *J. Phys. Chem. A* **2014**, *118*, 8264−8269.
(23) Nimmala, P. R.; Knoppe, S.; Jupally, V. R.; Delcamp, J. H.; Aikens, C. M.; Dass, A. *J. Phys. Chem. B* **2014**, *118*, 14157−14167.
(24) Azubel, M.; Koivisto, J.; Malola, S.; Bushnell, D.; Hura, G. L.; Koh, A. L.; Tsunoyama, H.; Tsukuda, T.; Pettersson, M.; Häkkinen, H.; Kornberg, R. D. *Science* **2014**, *345*, 909−912.
(25) Dainese, T.; Antonello, S.; Gascón, J. A.; Pan, F.; Perera, N. V.; Ruzzi, M.; Venzo, A.; Zoleo, A.; Rissanen, K.; Maran, F. *ACS Nano* **2014**, *8*, 3904−3912.
(26) Tlahuice-Flores, A.; Whetten, R. L.; Jose-Yacaman, M. *J. Phys. Chem. C* **2013**, *117*, 20867−20875.
(27) Whetten, R. L.; Khoury, J. T.; Alvarez, M. M.; Murthy, S.; Vezmar, I.; Wang, Z. L.; Stephens, P. W.; Cleveland, C. L.; Luedtke, W. D.; Landman, U. *Adv. Mater.* **1996**, *8*, 428−433.
(28) Whetten, R. L.; Shafigullin, M. N.; Khoury, J. T.; Schaaff, T. G.; Vezmar, I.; Alvarez, M. M.; Wilkinson, A. *Acc. Chem. Res.* **1999**, *32*, 397−406.
(29) Negishi, Y.; Chaki, N. K.; Shichibu, Y.; Whetten, R. L.; Tsukuda, T. *J. Am. Chem. Soc.* **2007**, *129*, 11322−11323.
(30) Chaki, N. K.; Negishi, Y.; Tsunoyama, H.; Shichibu, Y.; Tsukuda, T. *J. Am. Chem. Soc.* **2008**, *130*, 8608−8610.
(31) Negishi, Y.; Sakamoto, C.; Ohyama, T.; Tsukuda, T. *J. Phys. Chem. Lett.* **2012**, *3*, 1624−1628.
(32) Brust, M.; Walker, M.; Bethell, D.; Schiffrin, D. J.; Whyman, R. *J. Chem. Soc., Chem. Commun.* **1994**, 801−802.
(33) Yuan, X.; Yu, Y.; Yao, Q.; Zhang, Q.; Xie, J. *J. Phys. Chem. Lett.* **2012**, *3*, 2310−2314.
(34) Wolfe, R. L.; Murray, R. W. *Anal. Chem.* **2006**, *78*, 1167−1173.
(35) Negishi, Y.; Kurashige, W.; Niihori, Y.; Iwasa, T.; Nobusada, K. *Phys. Chem. Chem. Phys.* **2010**, *12*, 6219−6225.
(36) Negishi, Y.; Iwai, T.; Ide, M. *Chem. Commun.* **2010**, *46*, 4713−4715.
(37) Dass, A.; Stevenson, A.; Dubay, G. R.; Tracy, J. B.; Murray, R. W. *J. Am. Chem. Soc.* **2008**, *130*, 5940−5946.
(38) Negishi, Y.; Nobusada, K.; Tsukuda, T. *J. Am. Chem. Soc.* **2005**, *127*, 5261−5270.
(39) Mortensen, J. J.; Hansen, L. B.; Jacobsen, K. W. *Phys. Rev. B* **2005**, *71*, 035109.
(40) Enkovaara, J.; Rostgaard, C.; Mortensen, J. J.; Chen, J.; Dułak, M.; Ferrighi, L.; Gavnholt, J.; Glinsvad, C.; Haikola, V.; Hansen, H. A.; Kristoffersen, H. H.; Kuisma, M.; Larsen, A. H.; Lehtovaara, L.; Ljungberg, M.; Lopez-Acevedo, O.; Moses, P. G.; Ojanen, J.; Olsen, T.; Petzold, V.; Romero, N. A.; Stausholm-Møller, J.; Strange, M.; Tritsaris, G. A.; Vanin, M.; Walter, M.; Hammer, B.; Häkkinen, H.; Madsen, G. K. H.; Nieminen, R. M.; Nørskov, J. K.; Puska, M.; Rantala, T. T.; Schiøtz, J.; Thygesen, K. S.; Jacobsen, K. W. *J. Phys.: Condens. Matter.* **2010**, *22*, 253202.
(41) Perdew, J. P.; Wang, Y. *Phys. Rev. B* **1992**, *45*, 13244−13249.
(42) Casida, M. E.; Jamorski, C.; Bohr, F.; Guan, J.; Salahub, D. R. In *Recent Advances in Density Functional Methods*; ACS Press: Washington, D.C., 1996; p 145.
(43) Walter, M.; Häkkinen, H.; Lehtovaara, L.; Puska, M.; Enkovaara, J.; Rostgaard, C.; Mortensen, J. J. *J. Chem. Phys.* **2008**, *128*, 244101.
(44) Perdew, J. P.; Burke, K.; Ernzerhof, M. *Phys. Rev. Lett.* **1996**, *77*, 3865−3868.
(45) Lopez-Acevedo, O.; Akola, J.; Whetten, R. L.; Grönbeck, H.; Häkkinen, H. *J. Phys. Chem. C* **2009**, *113*, 5035−5038.
(46) Jadzinsky, P. D.; Calero, G.; Ackerson, C. J.; Bushnell, D. A.; Kornberg, R. D. *Science* **2007**, *318*, 430−433.
(47) Devadas, M. S.; Bairu, S.; Qian, H.; Sinn, E.; Jin, R.; Ramakrishna, G. *J. Phys. Chem. Lett.* **2011**, *2*, 2752−2758.
(48) Weissker, H.-Ch; Escobar, H. B.; Thanthirige, V. D.; Kwak, K.; Lee, D.; Ramakrishna, G.; Whetten, R. L.; López-Lozano, X. *Nat. Commun.* **2014**, *5*, 3785.
(49) Kreibig, U. *J. Phys.* **1977**, *38*, C2−97.
(50) Link, S.; El-Sayed, M. A. *J. Phys. Chem. B* **1999**, *103*, 4212−4217.
(51) Schaaff, T. G.; Shafigullin, M. N.; Khoury, J. T.; Vezmar, I.; Whetten, R. L. *J. Phys. Chem. B* **2001**, *105*, 8785−8796.
(52) Cleveland, C. L.; Landman, U.; Shafigullin, M. N.; Stephens, P. W.; Whetten, R. L. *Z. Phys. D* **1997**, *40*, 503−508.
(53) Lopez-Acevedo, O.; Tsunoyama, H.; Tsukuda, T.; Häkkinen, H.; Aikens, C. M. *J. Am. Chem. Soc.* **2010**, *132*, 8210−8218.
(54) Tlahuice-Flores, A.; Santiago, U.; Bahena, D.; Vinogradova, E.; Conroy, C. V.; Ahuja, T.; Bach, S. B. H.; Ponce, A.; Wang, G.; José-Yacamán, M.; Whetten, R. L. *J. Phys. Chem. A* **2013**, *117*, 10470−10476.
(55) Häkkinen, H.; Walter, M.; Grönbeck, H. *J. Phys. Chem. B* **2006**, *110*, 9927−9931.
(56) The structure proposed in ref 10 for $Au_{144}(SR)_{60}$ has the same Au_{114} core and the same Au−S connectivity at the metal−ligand interface as the model proposed by Lopez-Acevedo in ref 45 and is in fact just another rotamer of the same basic geometry.
(57) Malola, S.; Lehtovaara, L.; Enkovaara, J.; Häkkinen, H. *ACS Nano* **2013**, *7*, 10263−10270.

DOI: 10.1021/ja5109968
J. Am. Chem. Soc. 2015, 137, 1206−1212